Received 2 September 2024; Accepted 15 October 2024
https://doi.org/10.48612/letters/2024-4-319-324
https://elibrary.ru/whsxhi

# Grain boundary wetting phenomena in the Al-Cu system

B. B. Straumal†[1], O. A. Kogtenkova[1], A. N. Nekrasov[2], J. Dutta Majumdar[3],
G. Faraji[4], D. Bradai[5]

†straumal@issp.ac.ru

[1]Osipyan Institute of Solid State Physics, Russian Academy of Sciences, Chernogolovka 142432, Russia
[2]Korzhinskii Institute of Experimental Mineralogy, Russian Academy of Sciences, Chernogolovka 142432, Russia
[3]Department of Metallurgical and Materials Engineering, Indian Institute of Technology Kharagpur, Kharagpur 721302, India
[4]School of Mechanical Engineering, College of Engineering, University of Tehran, Tehran 11155 – 4563, Iran
[5]Faculty of Physics, University of Sciences and Technology Houari Boumediene, 16111 Algiers, Algeria

**Abstract:** The complete and incomplete wetting of (Al)/(Al) grain boundaries by the melt L is observed in the (Al)+L two-phase region of the Al-Cu phase diagram. Already slightly above the eutectic transformation temperature, approximately 20% of the (Al)/(Al) GBs in the polycrystal are completely wetted by the melt. Their fraction increases with increasing temperature and reaches 100% at a temperature of 600°C. Above this temperature, all (Al)/(Al) GBs remain completely wetted by the melt L. In the (Al)+$Al_2Cu$ two-phase region of the Al-Cu phase diagram the particles of the second solid phase $Al_2Cu$ (θ-phase) are observed in the (Al)/(Al) GBs and in the bulk. The $Al_2Cu$ precipitates form a nonzero (and rather large) contact angle with (Al)/(Al) GBs. Thus, the complete wetting of the (Al)/(Al) GBs by the second solid phase $Al_2Cu$ is not observed in the Al-Cu system. From this point of view, the Al-Cu alloys differ from the previously studied Al-Mg and Al-Zn alloys where the (Al)/(Al) GBs can be completely wetted by the second solid phase ($Al_3Mg_2$ and (Zn), respectively).

**Keywords:** phase transitions, grain boundaries, complete wetting, incomplete wetting, melt, solid phase

***Acknowledgement:*** *This research was funded by the Russian ministry of science and higher education (contract no. 075-15-2024-652 grant no. 13.2251.21.0252)*

## 1. Introduction

If you put a small amount of liquid on a large solid flat substrate, then two different situations are possible in principle. In the first case, the liquid forms small droplets on the substrate. In this case, the contact angle θ between the liquid surface and the substrate is not zero. This situation is called incomplete wetting. In the second case, the liquid completely spreads over the substrate. Then the contact angle θ is formally zero. This is a complete wetting of the substrate with liquid. In 1977, Cahn, as well as Ebner and Saam showed that with a change in temperature, a transition from incomplete to complete wetting is possible at a certain temperature $T_w$ [1,2]. Moreover, this transition at $T_w$ is, from a thermodynamic point of view, a true surface phase transition. Subsequently, the wetting phase transitions attracted a lot of attention from researchers [3]. In addition, it was found that wetting phase transitions can also occur at interfaces, in particular at grain boundaries (GBs) [4]. In the case of incomplete wetting (see diagram in Fig. 1a), the liquid phase forms separate droplets at GBs with a non-zero contact angle θ. In the case of complete GB wetting by the melt (see diagram in Fig. 1b), the liquid phase completely separates the solid grains from each other and θ = 0. It is essential that the second phase can be not only liquid, but also solid [5]. The thermodynamic scheme of incomplete and complete wetting does not differ for GB wetting by melt and by the second solid phase. However, the kinetics of achieving equilibrium is different. If the wetting phase is liquid, then equilibrium can be achieved within a few minutes. If the wetting phase is solid, then several months of annealing may be required to achieve equilibrium.

Subsequently, the GB wetting phase transitions became a popular object of research [6 – 8]. In particular, it was

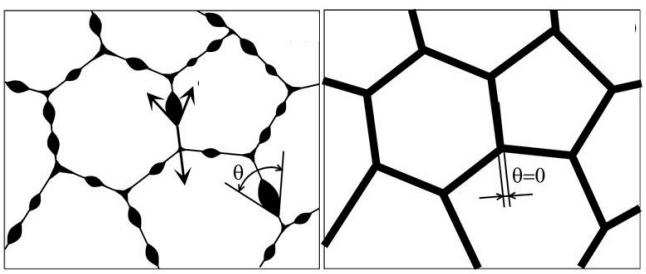


**Fig. 1.** A diagram showing incomplete and complete GB wetting by the second phase. With incomplete wetting (a), the second phase forms particles at the grain boundaries with a contact angle θ not equal to zero. In the case of complete wetting (b), the second phase is distributed along the boundaries and completely separates the grains of the matrix from each other. The contact angle in this case is θ = 0.

found that since the GB energy significantly depends on GB crystallographic parameters, the temperature $T_w$ of the wetting phase transition can vary in a wide range. Below a certain temperature of $T_{w\,min}$ (being minimum wetting phase transition temperature) all grain boundaries are incompletely wetted, but above the maximum wetting temperature of $T_{w\,max}$, all GBs are completely wetted, and grains are separated from each other by a liquid layer. In the range between $T_{w\,min}$ and $T_{w\,max}$, the portion of fully wetted GBs increases smoothly from zero to 100%. GB wetting phase transitions significantly affect a number of technological processes, such as severe plastic deformation and friction plunge welding [9,10]. Depending on how the second phase is distributed along the boundaries (in the form of particles or continuous layers), for example, the mechanical or magnetic properties of materials can also change [11,12]. Grain boundary wetting phenomena were observed in steels [13–15], in titanium-based alloys [16–18], in tin alloys [19,20], in copper alloys [21–24], in lithium alloys [25], in WC-Co cemented carbides [26,27], in magnesium alloys [11,28], in materials for permanent magnets based on the Nd-Fe-B system [12,29], as well as in multicomponent high-entropy alloys [30,31].

Aluminum-based alloys play a special role in modern technologies. They are used in a huge variety of products. It is not surprising that the phenomenon of GB wetting has been studied in detail in aluminum-based alloys [32–34], in Al-Zn alloys [35–42], including those after severe plastic deformation, as well as in Galfan Zn-5 wt.% Al alloys for the protective coatings [5,43–49]. At the same time, aluminum-copper alloys have not been studied sufficiently [50,51]. Only the "wormlike coarse $Al_2Cu$ particles" were observed in the annealed Al-33.2 wt.% Cu alloy modified with γ-$Al_2O_3$ [50] or $ZrB_2$ particle clusters [51]. Therefore, the purpose of this work was to study the GB wetting in the aluminum-copper system, both by melt and by the second solid phase of $Al_2Cu$ (θ-phase, see the phase diagram in Fig. 2 a).

## 2. Materials and methods

The Al-Cu alloys with 1, 2, 4 and 6 wt.% Cu (Fig. 2) were prepared from the high-purity 5N Al and 5N5 Cu using the vacuum induction melting. The ∅10 mm cylindrical Al-Cu ingots were cut using the spark erosion into 2 mm thick disks. Each disk was sealed into evacuated silica ampoule with a residual pressure of approximately $4\times10^{-4}$ Pa. Samples were annealed at temperatures between 300 and 610°C (see experimental points in the Al-Cu phase diagram, Fig. 2). The accuracy of the annealing temperature was ±2°C. Green circles between 550 and 610°C in Fig. 2 show the experimental points in the (Al)+L area of the phase diagram. These samples were annealed for 15 min each and then quenched in water at 20°C. Red circles between 300 and 500°C in Fig. 2 show the experimental points in the area of the phase diagram where solid solution (Al) and the second solid θ-phase $Al_2Cu$ are in equilibrium. These samples were subjected to long-term annealing (for 2000 h at 400°C and for 600 h at 610°C), and then quenched in water. After quenching, samples were embedded in resin. Then they were mechanically ground and polished for the metallographic study, using 1 μm diamond paste for the last polishing step. The samples were

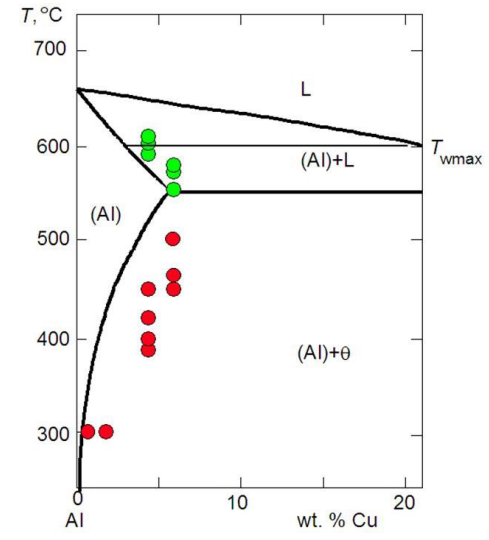


a

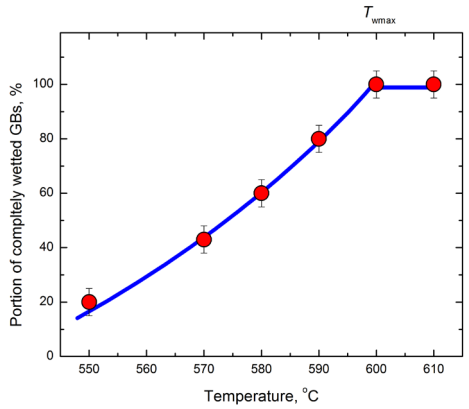


b

**Fig. 2.** (Color online) A section of the aluminum-copper phase diagram for aluminum-rich alloys (a). The experimental points for annealing in the region of the phase diagram, where the solid solution (Al) and the solid $Al_2Cu$ θ-phase are in equilibrium, are shown by red circles. The experimental points in the region of the phase diagram, where the aluminum-based solid solution (Al) and the melt L are in equilibrium, are shown by green circles. Solid thick lines show the boundaries of the existence of bulk phases. A thin horizontal tie-line at $T_{w\,max}$ = 600°C shows the maximum temperature of the grain boundary wetting phase transition. Above $T_{w\,max}$ the alloy contains completely wetted grain boundaries. Temperature dependence of the fraction of (Al)/(Al) grain boundaries completely wetted by the copper-containing melt (b).

investigated using scanning electron microscopy (SEM) or (after additional etching) by means of the light microscopy (LM). SEM characterization has been carried out on a Vega TS5130 MM (Tescan) microscope equipped with the LINK energy-dispersive spectrometer (Oxford Instruments). The energy-dispersive spectroscopy was used to determine the composition in various points of the annealed and quenched samples. Light microscopy has been performed using Neophot-32 LM equipped with 10 Mpix Canon Digital Rebel XT camera. The quantification of the grain boundary wetting transition was performed adopting the following criterion. Each Al/Al GB was considered to be completely wetted if a layer of $Al_2Cu$ θ-phase had covered the whole GB. If the Al/Al GB contains the separated particles of $Al_2Cu$

θ-phase, the GB was regarded as an incompletely wetted. At least 100 GBs were analysed at each temperature. Typical micrographs obtained by SEM are shown in Figs. 3 and 4.

## 3. Results and discussion

### *3.1. Wetting of Al/Al GB by the Cu-rich melt*

Figure 3 shows micrographs of samples annealed above the temperature of eutectic decomposition of the melt L into a solid solution of copper in aluminum (Al) and intermetallic phase $Al_2Cu$ (θ-phase). The corresponding experimental points are indicated in Fig. 2 by green circles. The aluminum matrix (Al) looks dark in these micrographs, it contains a little amount of copper (see Table 1). The areas that were liquid during annealing look light in the micrographs in Fig. 3. They contain an amount of copper that approximately corresponds to the composition of the melt on the liquidus line during annealing (see Table 1). During quenching, these areas solidified in accordance with the eutectic reaction $L \rightarrow (Al) + Al_2Cu$. Therefore, at high magnification (Fig. 3 d), it is clearly visible that they are fine-crystalline eutectic containing $Al_2Cu$ intermetallic phase, which looks light, and small plates of solid solution (Al).

After annealing at a temperature of 550°C (Fig. 3 a), slightly exceeding the temperature of the eutectic transformation, the melt consisted of equiaxed particles in the volume of (Al) grains, as well as elongated lenticular particles in the grain boundaries (Al)/(Al). These GBs were not completely wetted. In addition, the continuous melt layers are located at some (Al)/(Al) boundaries. These GBs were completely wetted by the melt. In Fig. 3 b, the symbols PW and CW show, respectively, such partially and completely wetted GBs. Thus, the GBs completely wetted by the melt, although in small portion, appear in the sample already at a temperature almost identical to the eutectic one. This means that in the aluminum-copper system, it is impossible to plot a minimum wetting phase transition tie-line at $T_{w\min}$ in the phase diagram, below which only incompletely wetted boundaries are observed in the polycrystal. After annealing at a temperature of 580°C (Fig. 3 b), the number of completely wetted GBs increases, and the number of partially wetted boundaries decreases compared to a temperature of 550°C. At a temperature of 600°C (Fig. 3 c, d), all grain boundaries are completely wetted by the melt, and the number of melt particles in the grain volume is small.

Figure 2 b shows the temperature dependence of the fraction of grain boundaries (Al)/(Al) completely wetted by the melt containing copper. This portion increases with increasing temperature from about 20% at 550°C to 100% at 600°C. Thus, starting from this temperature and above it, all (Al)/(Al) GBs are completely wetted by the melt. This means that the $T_{w\max}$ temperature in this system is 600°C.

Thus, we observe that the portion of completely wetted Al/Al GBs in the aluminum-copper system increases with increasing temperature until it reaches 100% at a temperature of 600°C. The transition from incomplete GB wetting by the melt to the complete one, as a rule, occurs with increasing temperature (as for example in aluminum-tin [52], copper-indium [53] or zinc-tin [20] systems). This is due to the fact

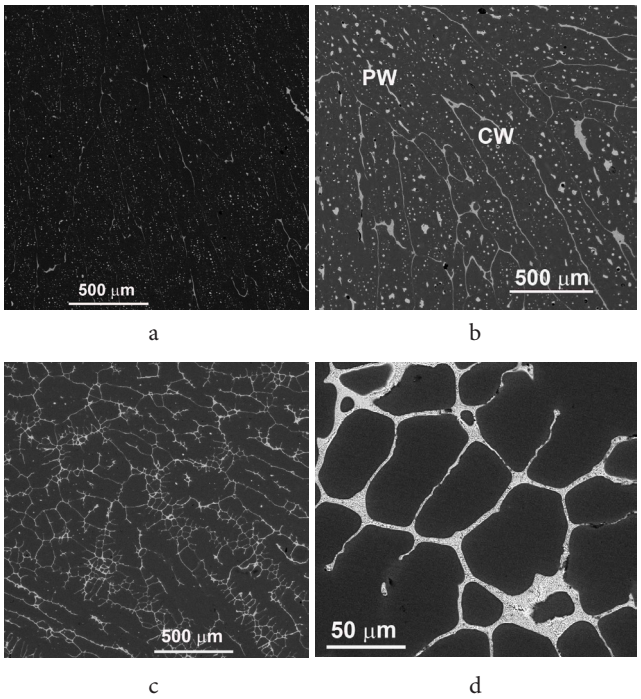


**Fig. 3.** SEM micrographs of Al-Cu samples annealed above the temperature of eutectic decomposition of the melt L into a solid solution of copper in aluminum (Al) and intermetallic $Al_2Cu$ (θ-phase). 550°C (a), 580°C (b), 600°C (c, d). The aluminum matrix (Al) looks dark in these micrographs, and the areas that were liquid during annealing look light in micrographs. During quenching, these areas solidified in accordance with the eutectic reaction $L \rightarrow (Al) + Al_2Cu$. Therefore, at high magnification (Fig. 3 d), it can be seen that they are a fine-plate eutectic made of $Al_2Cu$ intermetallic phase, which looks light, and small plates of solid solution (Al). The symbols in Fig. 3 b show partially (PW) and completely wetted (CW) GBs.

**Table 1.** Concentration of copper in the (Al) solid solution and in the Cu-rich GB layers in the Al-4 wt.% Cu alloy after annealing at 610°C.

| Temperature, °C | Cu content in (Al), wt.% | Cu content in GB layers, wt.% |
|---|---|---|
| 610 | 2 | 34 |

that the entropy of the melt is always higher than the entropy of the solid phase. Therefore, the temperature dependence of the free energy of the two interfaces between the solid and liquid phases decreases with increasing temperature faster than the GB free energy. This means that GBs coexist in equilibrium contact with the melt at lower temperatures and disappear, being replaced by a melt layer, with increasing temperature.

We observed earlier that the portion of GBs completely wetted by the melt increases with increasing temperature in polycrystals of copper-silver [54], copper-cobalt [55], copper-indium [53], aluminum-zinc [24], aluminum-magnesium [34], magnesium-REM (ZEK100 alloy [11] and EZ33A alloy [56]), NdFeB [29]. At the same time, in most of these systems, both the maximum $T_{w\max}$ and the minimum GB wetting transition temperature $T_{w\min}$ were observed [11, 24, 34, 53 – 56]. In this case, when a melt appears in the system with an increase in temperature, at first there are no completely wetted GBs below $T_{w\min}$. In this work, we observe that already just above the eutectic temperature of 550°C, the

completely wetted GBs immediately appear in polycrystals, about 20% of them (see Fig. 2b). From this point of view, the Al-Cu system resembles the NdFeB-based alloys [29] and EZ33A alloy [56], where, too, after crossing the eutectic temperature the completely wetted GBs immediately appear. From the thermodynamic point of view, it means that the energy of solid/liquid interphase boundaries is especially low, and the high-energy GBs become completely wetted already by the first portions of the melt.

### *3.2. Wetting of Al/Al GB by the second solid θ-phase $Al_2Cu$*

Figure 4 shows micrographs of samples annealed below the temperature of eutectic decomposition of the melt L into a solid solution of copper in aluminum (Al) and intermetallic phase $Al_2Cu$ (θ-phase). The corresponding experimental points are indicated in Fig. 2 by red circles. The aluminum matrix (Al) looks dark in these micrographs, it contains from 1 to 6 wt.% Cu (see Table 2). This concentration follows the solvus line in the Al-Cu phase diagram (Fig. 2). The areas of the $Al_2Cu$ (θ-phase) look light in the micrographs in Fig. 4. The concentration of copper in θ-phase after annealing at different temperatures is given in Table 3. At low temperatures the area of existence of intermetallic $Al_2Cu$ phase is very narrow, and it contains exactly 33.1 at.% Cu at 390°C. Close to the eutectic temperature, the area of existence of intermetallic $Al_2Cu$ phase becomes broader. Therefore, it contains 32.2 at.% Cu at 460°C and 32.0 at.% Cu at 500°C (see Table 3).

**Table 2.** Concentration of copper in the (Al) solid solution after annealing at different temperatures.

| Annealing temperature, °C | 300 | 390 | 400 | 420 | 450 | 460 | 500 |
|---|---|---|---|---|---|---|---|
| Cu content in (Al), wt.% | 1.1 | 2.1 | 2.4 | 2.5 | 3.4 | 4.8 | 6.2 |

**Table 3.** Concentration of copper in the GB layers of θ-phase after annealing at different temperatures.

| Temperature, °C | 390 | 460 | 500 |
|---|---|---|---|
| Cu content in θ-phase, wt.% | 53.3 | 52.8 | 52.6 |
| Cu content in θ-phase, at.% | 33.1 | 32.2 | 32.0 |

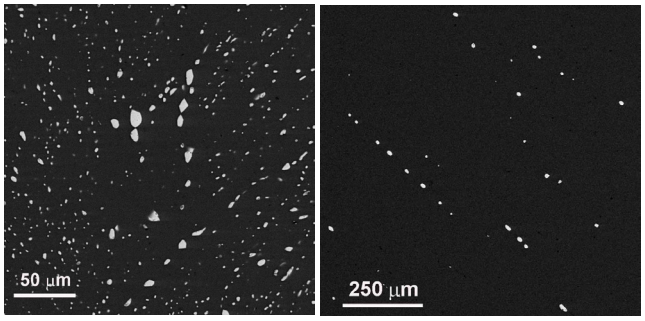


a b

**Fig. 4.** SEM micrographs of Al-Cu samples annealed below the temperature of eutectic decomposition of the melt L into a solid solution of copper in aluminum (Al) and intermetallic $Al_2Cu$ (θ-phase). Al-4 wt.% Cu alloy, 400°C (a), Al-6 wt.% Cu alloy, 600°C (b). The aluminum matrix (Al) looks dark in these micrographs, and the areas of the $Al_2Cu$ (θ-phase) look light in micrographs.

θ-phase particles are present both in the grain volume and in the (Al)/(Al) GBs. When the annealing temperature increases, the number of particles in the grain volume decreases. The particles in the volume are rounded having almost spherical shape. The particles in GBs are elongated and have almost spherical lenticular shape. The contact angle that the θ-phase particles form with the (Al)/(Al) GBs is not zero. It is quite large and varies slightly with the annealing temperature. This means that in the studied temperature range, there is no complete wetting of the (Al)/(Al) GBs by the second solid phase. Thus, in the two-phase region of the volumetric phase diagram aluminum-copper (Fig. 2a) there are no new lines for wetting phase transitions of grain boundaries (Al)/(Al) by the second solid phase $Al_2Cu$.

Thus, the aluminum-copper system differs significantly from the previously studied aluminum-zinc and aluminum-magnesium alloys in terms of GB wetting by the second solid phase [24, 57, 58]. For example, in the Al-Mg alloys, the second solid phase $Al_3Mg_2$ can completely wet (Al)/(Al) GBs [24, 57]. At temperatures below $T_{w\,min} = 220$°C, there are no (Al)/(Al) GBs completely wetted with the second solid phase in the Al-Mg polycrystals. The fraction of completely wetted (Al)/(Al) GBs increases with increasing temperature and reaches 100% at 410°C. At temperatures above $T_{w\,max} = 410$°C, all (Al)/(Al) GBs are completely wetted with the second solid phase $Al_3Mg_2$. In the Al-Zn system, on the contrary, at higher temperatures above $T_{w\,min} = 205$°C, there are no (Al)/(Al) GBs completely wetted with the second solid phase (Zn) [24, 57]. They appear at temperatures below $T_{w\,min} = 205$°C. Their fraction, on the contrary, increases with decreasing temperature and reaches 100% at $T_{w\,max} = 125$°C. We should also underline that the amount of second phase (liquid or solid) does not change the thermodynamic conditions for the complete or partial GB wetting. However, if the amount of the wetting phase is high, its layer can surround the matrix grains even if the contact angles are small but non-zero [53]. This phenomenon was called the apparently complete wetting [53]. However, it is not our case in this work since the experimental points (Fig. 2) are quite close to the solidus and solvus lines and, therefore, the portion of the wetting phase is low.

## 4. Conclusions

In the Al-Cu system, the complete and incomplete wetting of (Al)/(Al) grain boundaries by the melt L. is observed. In the (Al)+L two-phase region of the Al-Cu phase diagram, already slightly above the eutectic transformation temperature, approximately 20% of the (Al)/(Al) GBs in the polycrystal are completely wetted by the melt. Their fraction increases with increasing temperature and reaches 100% at a temperature of 600°C. Above this temperature, all (Al)/(Al) GBs remain completely wetted by the melt L.

In the (Al)+$Al_2Cu$ two-phase region of the Al-Cu phase diagram the particles of the second solid phase $Al_2Cu$ (θ-phase) are observed in the (Al)/(Al) GBs and in the bulk. The $Al_2Cu$ precipitates form a nonzero (and rather large) contact angle with (Al)/(Al) GBs. Thus, the complete wetting of the (Al)/(Al) GBs by the second solid phase $Al_2Cu$ is not observed in the Al-Cu system.

## References


1. J.W. Cahn, Critical point wetting, J. Chem. Phys. 66 (1977) 3667 – 3676.
2. C. Ebner, W.F. Saam, New phase-transition phenomena in thin argon films, Phys. Rev. Lett. 38 (1977) 1486 –1489.
3. D. Bonn, J. Eggers, J. Indekeu, J. Meunier, E. Rolley, Wetting and spreading, Rev. Mod. Phys. 81 (2009) 739 – 805.
4. E.I. Rabkin, L.S. Shvindlerman, B.B. Straumal, Grain boundaries: Phase transitions and critical phenomena, Int. J. Mod. Phys. B 5 (1991) 2989 – 3028.
5. G.A. López, E.J. Mittemeijer, B.B. Straumal, Grain boundary wetting by a solid phase; microstructural development in a Zn-5 wt.% Al alloy, Acta Mater. 52 (2004) 4537 – 4545.
6. J. Wang, L. Han, X. Li, D. Liu, L. Luo, Y. Huang, Y. Liu, Z. Wang, Supermodulus effect by grain-boundary wetting in nanostructured multilayers, J. Mater. Sci. Technol. 65 (2021) 202 – 209.
7. P. Wynblatt, D. Chatain, Y. Pang, Some aspects of the anisotropy of grain boundary segregation and wetting. J Mater Sci 41 (2006) 7760 – 7768.
8. P. Garg, T.J. Rupert, Grain incompatibility determines the local structure of amorphous grain boundary complexions, Acta Mater. 244 (2023) 118599.
9. Z. Zhang, D, Liu, Y. Wang, Y. Pang, F. Zhang, Y. Yang, J. Wang, A novel method for preparing bulk ultrafine-grained material: Three dimensional severe plastic deformation, Mater. Lett. 276 (2020) 128209.
10. Z. Zhao, K. Xiao, D. Wang, M. Hu, X. Ding, Aging effect on microstructure and properties of SAC305/Cu column interconnect obtained by friction plunge welding, Mater. Lett. 271 (2020) 127779.
11. B. Straumal, N. Khrapova, A. Druzhinin, K. Tsoy, G. Davdian, V. Orlov, G. Gerstein, A. Straumal, Grain boundary wetting transition in the Mg-based ZEK 100 alloy, Crystals 13 (2023) 1538.
12. A. Mazilkin, B.B. Straumal, S.G. Protasova, S. Gorji, A.B. Straumal, M. Katter, G. Schütz, B. Baretzky, Grain boundary oxide layers in NdFeB-based permanent magnets, Mater. Design 199 (2021) 109417.
13. M. Günen, A. Bakkaloğlu, Influence of sinter-hardening on microstructures and mechanical properties of Astaloy Mo-based steels, Mater. Lett. 251 (2019) 201 – 205.
14. M.I. Abdulsalam, Study of simulated disbonded polymer film on Zn-Al alloy coated reinforcing steel rebars, Corr. Sci. 138 (2018) 307 – 318.
15. O.I. Noskovich, E.I. Rabkin, V.N. Semenov, B.B. Straumal, L.S. Shvindlerman, Wetting and premelting phase transitions in 38° [100] tilt grain boundaries in (Fe-12at.%Si) Zn alloy in the vicinity of the A2-B2 bulk ordering in Fe-12 at.% Si alloy. Acta metall. mater. 39 (1991) 3091 – 3098.
16. S. Shukla, V. Bajpai, Effect of cryogenic quenching on microstructure and microhardness of Ti-6Al-4V alloy. Mater. Lett. 267 (2020) 127532.
17. X. Huang, Y. Feng, J. Ge, X. Meng, Y. Wang, L. Li, Z. Li, M. Ding, Electron irradiation mechanism of $Ti_3AlC_2$ material by in situ observation, Mater. Lett. 262 (2020) 127061.
18. A.S. Gornakova, S.I. Prokofiev, B.B. Straumal, K.I. Kolesnikova, Growth of (αTi) grain boundary layers in Ti-Co alloys, Russ. J. Non-Ferr. Met. 57 (2016) 703 – 709.
19. W.C. Ting, H. Yong, T.G. Langdon, The significance of strain weakening and self-annealing in a superplastic Bi-Sn eutectic alloy processed by high-pressure torsion, Acta Mater. 185 (2020) 245 – 256.
20. B.B. Straumal, W. Gust, T. Watanabe, Tie lines of the grain boundary wetting phase transition in the Zn-rich part of the Zn-Sn phase diagram, Mater. Sci. Forum 294/296 (1999) 411 – 414.
21. S. Gorsse, B. Ouvrard, M. Gouné, A. Poulon-Quintin, Microstructural design of new high conductivity – high strength Cu-based alloy, J. Alloys Compd. 633 (2015) 42 – 47.
22. S. Shu, X. Zhang, P. Bellon, R.S. Averback, Non-equilibrium grain boundary wetting in Cu-Ag alloys containing W nanoparticles, Mater. Res. Lett. 4 (2016) 22 – 26.
23. L.-S. Chang, B.B. Straumal, E. Rabkin, W. Gust, F. Sommer, The solidus line of the Cu-Bi phase diagram, J. Phase Equil. 18 (1997) 128 –135.
24. B.B. Straumal, O.A. Kogtenkova, A.B. Straumal, B. Baretzky, Grain boundary wetting-related phase transformations in Al and Cu-based alloys, Lett. Mater. 8 (2018) 364 – 371.
25. G. Wang, D. Song, C. Li, E.E. Klu, Y. Qiao, J. Sun, J. Jiang, A. Ma, Developing improved mechanical property and corrosion resistance of Mg-9Li alloy via solid-solution treatment, Metals 9 (2019) 920.
26. B.B. Straumal, I. Konyashin, B. Ries, A.B. Straumal, A.A. Mazilkin, K.I. Kolesnikova, A.M. Gusak, B. Baretzky, Pseudopartial wetting of WC/WC grain boundaries in cemented carbides, Mater. Lett. 147 (2015) 105 –108.
27. A.A. Mazilkin, B.B. Straumal, S.G. Protasova, M.F. Bulatov, B. Baretzky, Pseudopartial wetting of W/W grain boundaries by the nickel-rich layers, Mater. Lett. 192 (2017) 101–103.
28. B. Straumal, K. Tsoy, A. Druzhinin, V. Orlov, N. Khrapova, G. Davdian, G. Gerstein, A. Straumal, Coexistence of intermetallic complexions and bulk particles in grain boundaries in the ZEK100 alloy, Metals 13 (2023) 1407.
29. B.B. Straumal, Yu.O. Kucheev, I.L. Yatskovskaya, I.V. Mogilnikova, G. Schütz, B. Baretzky, Grain boundary wetting in the NdFeB-based hard magnetic alloys, J. Mater. Sci. 47 (2012) 8352 – 8359.
30. X. Gao, Y. Lu, Laser 3D printing of CoCrFeMnNi high-entropy alloy, Mater. Lett. 236 (2019) 77 – 80.
31. P. Sreeramagiri, G. Balasubramanian, Directed energy deposition of multi-principal element alloys, Front. Mater. 9 (2022) 825276.
32. P. Zhao, Z. Li, Z. Xu, X. Leng, A. Tong, J. Yan, Migrating behaviors of interfacial elements and oxide layers during diffusion bonding of 6063Al alloys using Zn interlayer in air, J. Mater. Sci. Technol. 155 (2023) 119 –131.
33. A. Mochugovskiy, N. Tabachkova, A. Mikhaylovskaya, Annealing induced precipitation of nanoscale icosahedral quasicrystals in aluminum based alloy, Mater. Lett. 247 (2019) 200 – 203.

34. B. B. Straumal, O. A. Kogtenkova, M. Yu. Murashkin, M. F. Bulatov, T. Czeppe, P. Zięba, Grain boundary wetting transition in Al-Mg alloys. Mater. Lett. 186 (2017) 82 – 85.
35. N. Q. Chinh, P. Jenei, J. Gubicza, E. V. Bobruk, R. Z. Valiev, T. G. Langdon, Influence of Zn content on the microstructure and mechanical performance of ultrafine-grained Al-Zn alloys processed by high-pressure torsion, Mater. Lett. 186 (2017) 334 – 337.
36. A. Q. Ahmed, D. Ugi, J. Lendvai, M. Yu. Murashkin, E. V. Bobruk, R. Z. Valiev, N. Q. Chinh, Effect of Zn content on microstructure evolution in Al-Zn alloys processed by high-pressure torsion, J. Mater. Res. 38 (2023) 3602.
37. M. Xu, Z. Zheng, D. Han, R. Ma, A. Du, Y. Fan, X. Zhao, X. Cao, Wetting of liquid zinc-aluminum-magnesium alloy on steel substrate during hot-dipping: Understanding the role of the flux, Surf. Topogr.: Metrol. Prop. 10 (2022) 035038.
38. Y. R. Chen, Examination and analysis of 2 Pct Mg-55 Pct Al-1.6 Pct Si-Zn coating on steel, Metal. Mater. Trans. A 51 (2020) 5758 – 5770.
39. N. Q. Chinh, P. Szommer, J. Gubicza, M. El-Tahawy, E. V. Bobruk, M. Yu. Murashkin, R. Z. Valiev, Characterizing microstructural and mechanical properties of Al-Zn alloys processed by high-pressure torsion, Adv. Eng. Mater. 22 (2020) 1900672.
40. J. L. C. Quintana, S. S. Medina, M. Hernández, O. M. Suárez, Study of thermomechanical properties of an Al-Zn-based composite reinforced with dodecaboride particles, Adv. Mater. Sci. Eng. 2018 (2018) 2975234.
41. A. Baris, N. Q. Chinh, R. Z. Valiev, T. G. Langdon, Microstructure decomposition and unique mechanical properties in an ultrafine-grained Al-Zn alloy processed by high-pressure torsion, Kovove Mater. 53 (2015) 251 – 258.
42. B. B. Straumal, A. A. Mazilkin, X. Sauvage, R. Z. Valiev, A. B. Straumal, A. M. Gusak, Pseudopartial wetting of grain boundaries in severely deformed Al-Zn alloys, Russ. J. Non-Ferr. Met. 56 (2015) 44 – 51.
43. Y. Yuan, X. Liu, G. Pu, T. Wang, Q. Guo, Corrosion features and time-dependent corrosion model of Galfan coating of high strength steel wires, Constr. Build. Mater. 313 (2021) 125534.
44. N. Kalantarrashidi, M. Alizadeh, S. Pashangeh, Microstructure evolution and mechanical properties evolution of high-Zn Al-Zn alloys prepared by cross accumulative roll bonding combined with heat treatment process, J. Alloys Compd. 927 (2022) 167042.
45. T. Liu, R. Ma, Y. Fan, A. Du, X. Zhao, M. Wen, X. Cao, Effect of fluxes on wettability between the molten Galfan alloy and Q235 steel matrix, Surf. Coat. Technol. 337 (2018) 270 – 278.
46. X. Zhang, C. Leygraf, I. Odnevall Wallinder, Selected area visualization by FIB-milling for corrosion-microstructure analysis with submicron resolution, Mater. Lett. 98 (2013) 230 – 233.
47. X. Zhang, C. Leygraf, I. Odnevall Wallinder, Atmospheric corrosion of Galfan coatings on steel in chloride-rich environments, Corr. Sci. 73 (2013) 62 – 71.
48. X. Zhou, W. Shi, S. Xiang, Improving corrosion resistance of Zn-5Al wt.% alloy by microalloying with samarium, J. Rare Earths 41 (2023) 1636 –1644.
49. T. Gancarz, J. Pstrus, G. Cempura, K. Berent, Influence of Li addition to Zn-Al alloys on Cu substrate during spreading test and after aging treatment, J. Electron. Mater. 45 (2016) 6067 – 6078.
50. T. Gao, L. Liu, S. Liu, C. Yuan, Y. Bian, X. Liu, The growth behavior of $Al_2Cu$ phase in confined spaces constituted by γ-$Al_2O_3$ particle clusters, Mater. Lett. 304 (2021) 130711.
51. T. Gao, Y. Bian, L. Liu, K. Zhao, K. Hu, X. Liu, Modification of primary and eutectic phases in Al-33.2Cu and Al-20$Mg_2Si$ alloys by nano-treating, Mater. Lett. 286 (2021) 129218.
52. B. Straumal, W. Gust, D. Molodov, Wetting transition on the grain boundaries in Al contacting with Sn-rich melt, Interface Sci. 3 (1995) 127 –132.
53. A. B. Straumal, B. S. Bokstein, A. L. Petelin, B. B. Straumal, B. Baretzky, A. O. Rodin, A. N. Nekrasov, Apparently complete grain boundary wetting in Cu-In alloys. J. Mater. Sci. 47 (2012) 8336 – 8343.
54. B. B. Straumal, B. S. Bokstein, A. B. Straumal, A. L. Petelin, First observation of a wetting transition in low-angle grain boundaries, JETP Letters 88 (2008) 537 – 542.
55. B. B. Straumal, O. A. Kogtenkova, A. B. Straumal, Yu. O. Kuchyeyev, B. Baretzky, Contact angles by the solid-phase grain boundary wetting in the Co-Cu system. J. Mater. Sci. 45 (2010) 4271 – 4275.
56. A. B. Straumal, K. V. Tsoy, I. A. Mazilkin, A. N. Nekrasov, K. Bryła, Grain boundary wetting and material performance in an industrial EZ33A Mg cast alloy, Arch. Metall. Mater. 64 (2019) 869 – 873.
57. O. A. Kogtenkova, P. Zieba, T. Czeppe, L. Litynska-Dobrzynska, B. B. Straumal, A. N. Nekrasov, Wetting of grain boundaries by the second solid phase in the Al-based alloys. Bull. Russ. Ac. Sci. Phys. 77 (2013) 1386 –1390.
58. S. G. Protasova, O. A. Kogtenkova, B. B. Straumal, P. Zięba, B. Baretzky, Inversed solid-phase grain boundary wetting in the Al-Zn system, J. Mater. Sci. 46 (2011) 4349 – 4353.